

# Rigorous electromagnetic analysis of two dimensional micro-axicon by boundary integral equations

Jie Lin<sup>1,\*</sup>, Jiubin Tan<sup>1</sup>, Jian Liu<sup>1</sup>, and Shutian Liu<sup>2</sup>

<sup>1</sup>Harbin Institute of Technology, Center of Ultra-precision Optoelectronic Instrument, P.O. Box 718, Harbin 150001, CHINA

<sup>2</sup>Department of Physics, Harbin Institute of Technology, Harbin 150001, China

[linjie@hit.edu.cn](mailto:linjie@hit.edu.cn)

**Abstract:** The focal performance of the micro-axicon and the Fresnel axicon (fraxicon) are investigated, for the first time, by the rigorous electromagnetic theory and boundary element method. The micro-axicon with different angle of apex and the fraxicon with various period and angle of apex are investigated. The dark segments of the fraxicon are explored numerically. Rigorous results of focal performance of the micro-axicon and the fraxicon are different from the results given by the approximation of geometrical optics and the scalar diffraction theory. The scattering effects are dominant in the fraxicon with small size of feature. It is expected that our study can provide very useful information in analyzing the axicon in optical trapping systems.

© 2008 Optical Society of America

**OCIS codes:** (050.1970) Diffractive optics; (260.1960) Diffraction theory; (230.3990) Micro-optical devices.

---

## References and links

1. J. H. McLeod, "The axicon: a new type of optical element," *J. Opt. Soc. Am.* **44**, 592–597 (1954).
2. J. H. McLeod, "Axicons and their uses," *J. Opt. Soc. Am.* **50**, 166–169 (1960).
3. I. Golub and R. Tremblay, "Light focusing and guiding by an axicon-pair-generated tubular light beam," *J. Opt. Soc. Am. B* **7**, 1264–1267 (1990).
4. Y. Qian and Y. Z. Wang, "Theoretical analysis of a collimated hollow-laser-beam generated by a single axicon using diffraction integral," *Chin. Opt. Lett.* **2**, 232–234 (2004).
5. J. Fan, E. Parra and H. M. Milchberg, "Resonant self-trapping and absorption of intense Bessel beams," *Phys. Rev. Lett.* **84**, 3085–3088 (2000).
6. D. McGloin and K. Dholakia, "Bessel beams: diffraction in a new light," *Contemp. Phys.* **46**, 15–28 (2005).
7. V. V. Kotlyar, A. A. Kovalev, V. A. Soifer, C. S. Tuvey and J. A. Davis, "Sidelobe contrast reduction for optical vortex beams using a helical axicon," *Opt. Lett.* **32**, 921–923 (2007).
8. O. Brzobohatý, T. Čižmár and P. Zemánek, "High quality quasi-Bessel beam generated by round-tip axicon," *Opt. Express* **16**, 12688–12700 (2008).
9. M. Florjanczyk and R. Tremblay, "Guiding of atoms in a travelling-wave laser trap formed by the axicon," *Opt. Commun.* **74**, 448–450 (1989).
10. R. Arimoto, C. Saloma, T. Tanaka and S. Kawata, "Imaging properties of axicon in a scanning optical system," *Appl. Opt.* **31**, 6653–6657 (1992).
11. T. Tanaka and S. Yamamoto, "Comparison of aberration between axicon and lens," *Opt. Commun.* **184**, 113–118 (2000).
12. P.-A. Bélanger and M. Rioux, "Ring pattern of a lens-axicon doublet illuminated by a Gaussian beam," *Appl. Opt.* **17**, 1080–1088 (1978).

13. Z. Ding, H. Ren, Y. Zhao, J. S. Nelson and Z. Chen, "High-resolution optical coherence tomography over a large depth range with an axicon lens," *Opt. Lett.* **27**, 243–245 (2002).
14. D. J. Fischer, C. J. Harkrider and D. T. Moore, "Design and manufacture of a gradient-index axicon," *Appl. Opt.* **39**, 2687–2694 (2000).
15. J. Monsoriu, G. Saavedra and W. Furlan, "Fractal zone plates with variable lacunarity," *Opt. Express* **12**, 4227–4234 (2004).
16. I. Golub, "Fresnel axicon," *Opt. Lett.* **31**, 1890–1892 (2006).
17. J. A. Monsoriu, C. J. Zapata-Rodríguez and W. D. Furlan, "Fractal axicons," *Opt. Commun.* **263**, 1–5 (2006).
18. A. Burvall, P. Martinsson and A. Friberg, "Communication modes applied to axicons," *Opt. Express* **12** 377–383 (2004).
19. C.J. Zapata-Rodríguez, and F.E. Hernández, "Focal squeeze in axicons," *Opt. Commun.* **254**, 3–9 (2005).
20. L. Lin, S. Lee, K. Pister, M.C. Wu, "Three-dimensional micro-Fresnel optical elements fabricated by micromachining technique," *Electron. Lett.* **30**, 448–449 (1994).
21. W. C. Cheong, B. P. S. Ahluwalia, X.-C. Yuan, L.-S. Zhang, H. B. Niu, X. Peng, "Fabrication of efficient microaxicon by direct electron-beam lithography for long nondiffracting distance of Bessel beams for optical manipulation," *Appl. Phys. Lett.* **87**, 024104-1–3 (2005).
22. B. P. S. Ahluwalia, W. C. Cheong, X.-C. Yuan, L.-S. Zhang, S.-H. Tao, J. Bu, and H. Wang, "Design and fabrication of a double-axicon for generation of tailorable self-imaged three-dimensional intensity voids," *Opt. Lett.* **31**, 987–989 (2006).
23. K. Yashiro and S. Ohkawa, "Boundary element method for electromagnetic scattering from cylinders," *IEEE Trans. Antennas Propag.* **AP-33**, 383–389 (1985).
24. K. Hirayama, E. N. Glytsis, T. K. Gaylord and D. W. Wilson, "Rigorous electromagnetic analysis of diffractive cylindrical lenses," *J. Opt. Soc. Am. A* **13**, 2219–2231 (1996).
25. M. Bass, E. W. Van Stryland, D. R. Williams and W. L. Wolfe, "Handbooks of Optics, Vol. 2: Devices, Measurements and Properties," (McGraw-Hill, New York, 1995).

## 1. Introduction

An axicon, which was formally coined by J. H. McLeod [1, 2], is an optical element that images a point into a segment image along the optical axis instead of the usual point focus. The element has various practical applications such as beam generation, alignment, atom guiding, and scanning [3–11]. For example, a high-order Bessel beam can be generated by using of an axicon, which offers a reliable method for atom and nanoparticle guiding [5, 6]. An axicon combining with lens can produce various ring pattern along its optics axis [12]. The axicon can also be used as optics element with long focal depth using in alignment [13]. Therefore, the axicons and their derived elements are studied extensively in the recent years [14–17]. In the most cases, the focusing performance of the axicon can be investigated by using of the scalar diffraction theory, such as the Fresnel-Kirchoff diffraction integral [17–19]. With the development of processing technique, micro-axicon or the axicon with small feature size can be designed and manufactured [20–22].

For the micro-axicons or the axicons with small feature size, the diffraction and scattering will be enhanced as the decreasing in size, and their focusing performances are dominated by the scattering and diffraction effects generated on the boundaries. For example, in the case of the Fresnel axicon (fraxicon) and the fractal axicon, the focusing performance of the micro-axicon is governed by the scattering effect caused by the feature structure. Therefore, the scalar diffraction theory fails to solve the scattering and diffractive fields [18, 19], and the rigorous electromagnetic theory must be applied. Considering the great advantages in solving 2D finite-size scattering problem, the boundary integral equations and boundary element method (BEM) are used to calculate the focal characteristics of 2D micro optical elements [23, 24]. In this paper, we devote ourselves to investigate the focusing performance of the two-dimensional (2D) micro-axicon and fraxicon by rigorous electromagnetic theory. The focusing performance of the fraxicon with different number of zone is also investigated. The focal characteristics, such as the region field distribution and the intensity distribution along optical axis, are calculated in details. In Sec. 2, basic formulas of the boundary integral equations are described. In Sec. 3, we present the numerical results together with detailed analysis. A conclusion is given in Sec. 4.

## 2. Boundary integral equations

The schematic diagrams of the 2D micro-axicons and fraxicons are described in Fig. 1. The whole 2D space is divided into two semi-infinite regions, region  $S_1$  and region  $S_2$ , by axicon's boundary  $\Gamma$ . The region  $S_1$  is occupied by the 2D axicon with refractive index  $n_1$  and the region  $S_2$  usually is the air with the refractive index  $n_2=1.0$ . The 2D axicon is infinite along  $z$ -axis. A TE parallel beam is assumed incident along opposite direction of  $y$ -axis. After propagating through the axicon, the beams get interfered in region  $S_2$ . To calculate the optical field distributions in region  $S_2$ , the Green's theorem and Green function are applied to Maxwell's equations.

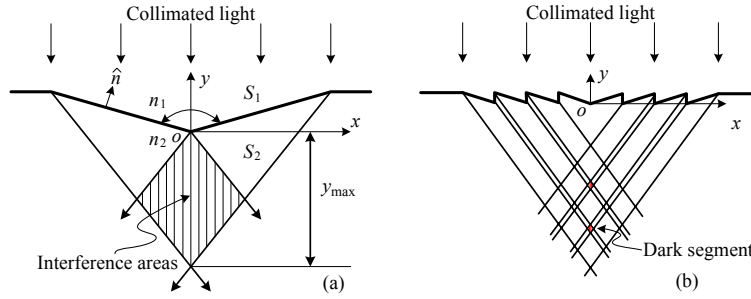


Fig. 1. A schematic diagram of axicons. (a) The bulk axicon, and (b) the Fresnel axicon with same angle of apex as given in (a).

By incorporating with Sommerfeld radiation condition, we can obtain the boundary integral equation about the boundary scattering fields and their normal derivatives. The boundary integral equations are discretized by using of the BEM. Through matrix inversion and Gaussian elimination method, the scattering fields and their normal derivatives can be determined. Therefore, the transmitted optical field in region  $S_2$  is computed numerically by [24]

$$\mathbf{E}(\mathbf{r}) = - \int_{\Gamma} \left[ \mathbf{E}_{\Gamma}(\mathbf{r}'_{\Gamma}) \frac{\partial G_2(\mathbf{r}, \mathbf{r}'_{\Gamma})}{\partial \hat{\mathbf{n}}} - G_2(\mathbf{r}, \mathbf{r}'_{\Gamma}) \frac{\partial \mathbf{E}_{\Gamma}(\mathbf{r}'_{\Gamma})}{\partial \hat{\mathbf{n}}} \right] dl', \quad (1)$$

where  $\mathbf{r}$  and  $\mathbf{r}'_{\Gamma}$  represent any point in region  $S_2$  and on micro-axicon boundary  $\Gamma$ , respectively.  $\mathbf{E}_{\Gamma}$  and  $\frac{\partial \mathbf{E}_{\Gamma}}{\partial \hat{\mathbf{n}}}$  indicate the boundary field and their normal derivative on the axicon boundary  $\Gamma$ , respectively, where  $\hat{\mathbf{n}}$  is normal to the boundary  $\Gamma$  with orientation to region  $S_1$ , as shown in Fig. 1(a).  $G_2$  is the 2D Green function in the region  $S_2$  and is described as a zeroth-order Hankel function of the second kind, i.e.,  $G_2(\mathbf{r}, \mathbf{r}'_{\Gamma}) = (-j/4)H_0^{(2)}(k_2|\mathbf{r} - \mathbf{r}'_{\Gamma}|)$ .  $k_2 = 2\pi n_2/\lambda$  is the wave number in the region  $S_2$ , and  $\lambda$  is the incident wavelength in free space.

## 3. Transmission characteristics of 2D micro-axicons

For the 2D bulk micro-axicon shown in Fig. 1(a), the geometry is governed by the refractive index of the material ( $n_1$ ), the size of the aperture ( $D = 2R$ ) and the angle of the apex ( $\theta$ ), where  $R$  is radial coordinate. The incident wavelength is  $\lambda = 1.0 \mu\text{m}$ . The micro-axicon and the fraxicon are assumed made of AIAs crystal and the refractive index is  $n_1 = 2.857$  at  $\lambda = 1.0 \mu\text{m}$  [25]. According to the principles of geometrical optics, the finite interference zone is given by  $y_{\text{max}} = R \tan \gamma - R \tan(\theta/2)$ , where  $2\gamma = \theta + 2\beta - \pi$ , and  $\beta = \arcsin[n_1 \cos(\theta/2)]$ , respectively. For a large apex angle,  $y_{\text{max}} \approx R \tan \gamma$ . However,  $y_{\text{max}}$  may fail to describe the focal performance when the scattering effect on the boundary of the micro-axicon is more obviously enhanced as the decreasing in the size of axicon. For the fraxicon, which is shown in Fig. 1(b), the dark segments caused by introducing the Fresnel zone will appear, and the

diffraction and scattering effects are more obviously if the feature size is approximately equal to the incident wavelength  $\lambda$ . When the collimated beam is propagating from the region  $S_1$  to the region  $S_2$ , the total reflection is occurred and the corresponding critical angle of apex is given as  $2 \arccos(1/n_1) \approx 139^\circ$ . In our work, the diameter of the 2D micro-axicons are  $50.0 \mu\text{m}$  and the angle of apex are chose as  $130^\circ$ ,  $140^\circ$ ,  $150^\circ$ ,  $160^\circ$ , and  $170^\circ$ , respectively.

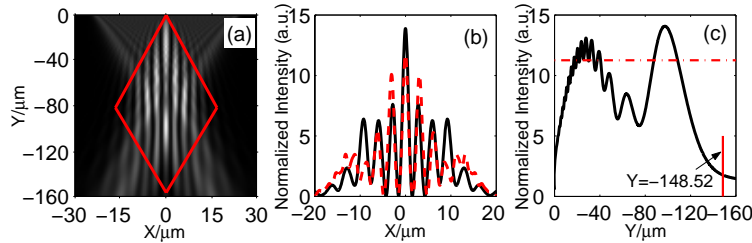


Fig. 2. The focal performance of 2D micro axicon with diameter  $D = 50.0 \mu\text{m}$  and angle of apex  $\theta = 170^\circ$ . (a) The gray-level intensity distributions in region  $S_2$ , (b) The lateral intensity distribution on different observation planes (solid curve for  $y = -100.0 \mu\text{m}$  and dashed curve for  $y = -40.0 \mu\text{m}$ , respectively), and (c) the intensity distribution along the axis of the micro-axicon.

We firstly investigate the focusing performance of micro-axicon with angle of apex  $\theta = 170^\circ$ . The gray-level representation of the electric-field distribution in the region  $S_2$  is drawn in Fig. 2(a), where the bright (dark) regions mark the locations with high (low) electric field intensities. The interference occurs in the region from  $y = 0$  to  $-148.52 \mu\text{m}$ . It is obviously seen that the interference fringes are parallel to the  $y$ -axis and occur in a rhombus-like region surrounded by the red lines. In this region, seven strong interference fringes appear in the marked region. In the large propagating range, the fringes keep parallel each other and the results can be seen in Fig. 2(b). The solid curve represents the lateral intensity distribution at  $y = -100.0 \mu\text{m}$ , while the red dashed curve for  $y = -40.0 \mu\text{m}$ . Along the propagation, the positions of the innermost five interference fringes are almost unchangeable and the distances between interference fringes are approximately constant. In fact, owing to the diffraction and scattering effects, blurry interference also appears in  $y = -148.52 \mu\text{m}$  to  $-160 \mu\text{m}$ , as shown in Fig. 2(a). Meanwhile, as

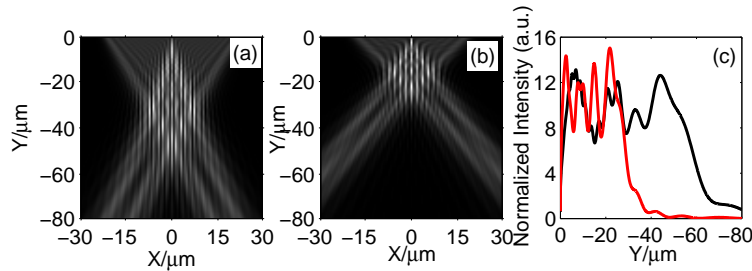


Fig. 3. Focal performance of the axicon with different angle of apex: (a) and (b) represent the field intensity distributions of the axicon with  $\theta = 160^\circ$  and  $150^\circ$  in the region  $S_2$ , respectively, and (c) displays the intensity profiles along  $y$ -axis.

shown in Fig. 2(c), the intensity distribution along  $y$ -axis is fluctuated. The dotted-dashed line is located at 80.0% maximum of the intensity. Obviously there are two ranges for the intensity larger than 80.0% maximum of the intensity. At  $y = -74.69 \mu\text{m}$ , an intensity well is formed, which disagrees with the result given by the scalar diffractive theory [6], and it can be used in

atom trapping. This characteristics can be attributed to the scattering on the boundary of the micro axicon. The local field intensity distributions of the axicon for  $\theta = 160^\circ$  and  $150^\circ$  are illustrated in Fig. 3(a) and (b), respectively. As the decreasing in the angle of apex, the interference fringes are located in a rhombus-like region and its shape is decayed. The theoretical ranges are  $y_{\max} = 65.25$  and  $32.27 \mu\text{m}$  for  $\theta = 160^\circ$  and  $150^\circ$ , respectively. In fact, as shown in Fig. 3(c), the ranges are reduced owing to the scattering effect and the intensity distribution is fluctuated in a range that is smaller than the range predicted by geometrical optics. When the angle of apex is smaller than the critical angle  $2\arccos(1/n_1)$ , weak power is transmitted into the region  $S_2$ .

With the decrease in feature size of the fraxicon, the focal characteristics is different comparing with the bulk axicon. In our work, the angle of apex is the same with that of bulk axicon, and the period of the fraxicon are chosen as  $T = 5.0$  and  $2.5 \mu\text{m}$ , respectively. Under the approximation of geometrical optics, the interference fringes along  $y$ -axis are not continuous: it consists of several dark segments which displays in Fig. 1(b). Furthermore, the number of the dark segments is equal to  $N - 1$ , where  $N = R/T$  is the number of Fresnel zones. For the fraxicon with  $T = 5.0$  and  $2.5 \mu\text{m}$ , the number of dark segments are 4 and 9, respectively. However, the numerical result departs from the results in the geometric optical approximation. In Fig. 4(a), several peaks appear on the intensity distributions on the observation plane  $y = -100.0 \mu\text{m}$ . It indicates that the interference caused by different Fresnel zones occurs in the region  $S_2$ . The position of interference has changed for the fraxicons. The interference occur in more positions for the smaller  $T$ . The much more obvious differences are easily seen from the axial intensity distributions. As shown in Fig. 4(b), for the fraxicon with  $T = 5.0 \mu\text{m}$ , only one obvious dark segment is emerged in the curve a at  $y = -40 \mu\text{m}$  nearby. For the fraxicon with  $T = 2.5 \mu\text{m}$ , five dark segments are observed in the curve b. It is obviously that the actual number of dark segments is much less than the predicted number.

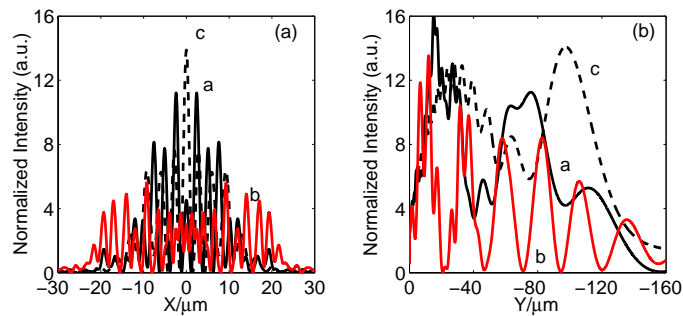


Fig. 4. (a) Normalized intensity distributions on observation plane  $y = -100.0 \mu\text{m}$ , and (b) the axial intensity distributions for different kinds of axicon. Curves a (black solid), b (red solid) and c (black dashed) describe the focal characteristics of the fraxicon with  $T = 5.0 \mu\text{m}$ ,  $T = 2.5 \mu\text{m}$  and the bulk axicon, respectively.

As the decreasing in the apex angle of the fraxicon, the number of dark segments changes. In our numerical results, as shown in Fig. 5(a), red arrows mark two positions that the intensity wells exist for the fraxicon with  $\theta = 170^\circ$ , which indicate there are two dark segments exist. With the further decrease of the apex angle, the positions of intensity wells will get increased, for instance, there are three dark segments for  $\theta = 160^\circ$ . For the cases of  $\theta = 150^\circ$  and  $140^\circ$ , number of dark segments are four. It is obviously that the number of dark segments is different for different angle of apex and the number is not monotonically changed with the angle of apex. According to the feature of fraxicon, the maximal thickness of each zone is increasing while

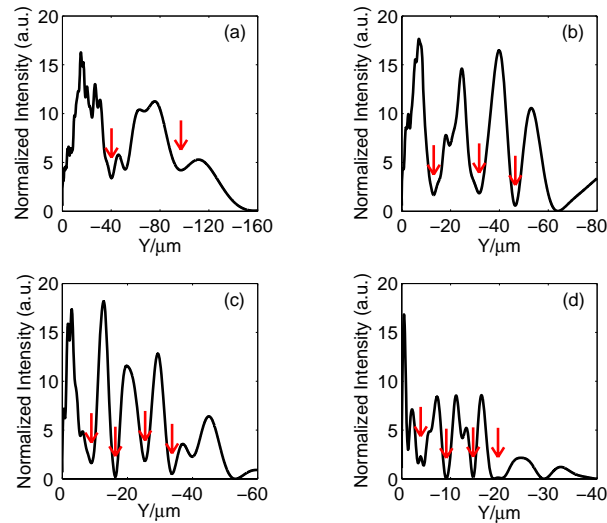


Fig. 5. The axial intensity distribution of  $T = 5.0 \mu\text{m}$  the fraxicon with different angle of apex. (a), (b), (c) and (d) are for  $\theta = 170^\circ$ ,  $160^\circ$ ,  $150^\circ$  and  $140^\circ$ , respectively. The red arrows mark the positions of dark segments.

the angle of apex is decreasing. That indicates the feature size of the fraxicon is increasing. Therefore the scattering of the fraxicon with small angle of apex is relatively weak compared with the fraxicon with large angle of apex. It is obviously that the focal performance of fraxicon is governed by scattering effect. The scattering effect is more evident as the decreasing in period of the fraxicon.

#### 4. Conclusion

The focal performance of the micro-axicon and the fraxicon have been analyzed by rigorous electromagnetic theory for the first time. The effect of the apex angle of the micro-axicon on focal performance has been numerically investigated. The focal characteristics of the fraxicon with different period and the angle of apex have been also numerically presented. Our study indicates that the rigorous results are different with the results given by the geometrical optics approximation and the scalar diffraction theory. With the decreasing in the angle of apex, the fluctuation on the axial intensity distribution is more acute. Dark segments are generated along axial intensity distribution. However, the number of dark segments is not equal to the results under the geometrical optics approximation. We found that the focal performance of the fraxicon is more sensitive to the period than the apex angle. For the fraxicon with same angle of apex, the scattering is more obvious in the case of small period. It is obviously significant that the rigorous electromagnetic theory are necessary to analyze the focal performance of micro-axicon and fraxicon with small feature size. It is expected that the rigorous numerical results may provide much useful information for the micro-axicon and the fraxicon used in micro-optics and optical trapping systems.

#### Acknowledgments

This work was supported by the National Natural Science Foundation of China under grants Nos. 60878028, 10674038 and 10604042 and National Basic Research Program of China under grant No. 2006CB302901.